LANGMUIR Article
Cite This: Langmuir 2019, 35, 10116−10127
pubs.acs.org/Langmuir

Phase Change Ultrasound Contrast Agents with a Photopolymerized Diacetylene Shell

Yosra Toumia,[†] Barbara Cerroni,[†] Fabio Domenici,[†] Heiko Lange,[†] Livia Bianchi,[†] Madalina Cociorb,[†] Francesco Brasili,[†] Ester Chiessi,[†] Emiliano D'Agostino,[‡] Koen Van Den Abeele,[§] Sophie V. Heymans,[§] Jan D'Hooge,[∥] and Gaio Paradossi*[,†]

[†]Department of Chemical Sciences and Technologies, University of Rome Tor Vergata, Via della Ricerca Scientifica 1, 00133, Rome, Italy

[‡]DoseVue NV, Philips Open Manufacturing Campus, Slachthuisstraat 96, B-2300 Turnhout, Belgium

[§]Department of Physics, KU Leuven, Kulak, 8500 Kortrijk, Belgium

[∥]Medical Center, KU Leuven, 3000 Leuven, Belgium

Supporting Information

ABSTRACT: Phase change contrast agents for ultrasound (US) imaging consist of nanodroplets (NDs) with a perfluorocarbon (PFC) liquid core stabilized with a lipid or a polymer shell. Liquid ↔ gas transition, occurring in the core, can be triggered by US to produce acoustically active microbubbles (MBs) in a process named acoustic droplet vaporization (ADV). MB shells containing polymerized diacetylene moiety were considered as a good trade off between the lipid MBs, showing optimal attenuation, and the polymeric ones, displaying enhanced stability. This work reports on novel perfluoropentane and perfluorobutane NDs stabilized with a monolayer of an amphiphilic fatty acid, i.e. 10,12-pentacosadiynoic acid (PCDA), cured with ultraviolet (UV) irradiation. The photopolymerization of the diacetylene groups, evidenced by the appearance of a blue color due to the conjugation of ene-yne sequences, exhibits a chromatic transition from the nonfluorescent blue color to a fluorescent red color when the NDs are heated or the pH of the suspension is basic. An estimate of the molecular weights reached by the polymerized PCDA in the shell, poly(PCDA), has been obtained using gel permeation chromatography and MALDI-TOF mass spectrometry. The poly(PCDA)/PFC NDs show good biocompatibility with fibroblast cells. ADV efficiency and acoustic properties before and after the transition were tested using a 1 MHz probe, revealing a resonance frequency between 1 and 2 MHz similar to other lipidic MBs. The surface of PCDA shelled NDs can be easily modified without influencing the stability and the acoustic performances of droplets. As a proof of concept we report on the conjugation of cyclic RGD and PEG chains of the particles to support targeting ability toward endothelial cells.

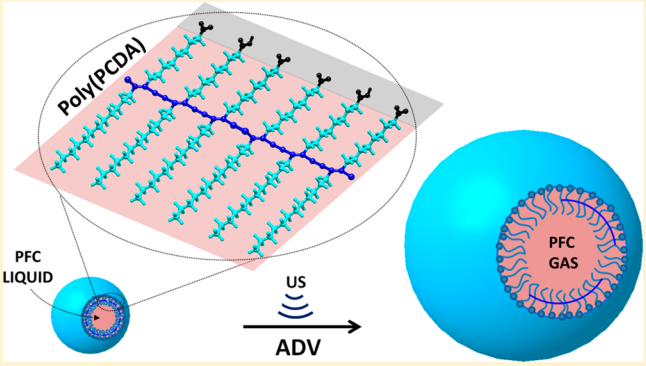

1. INTRODUCTION

Microbubbles (MBs) are micron-sized particles encapsulating a gas core and can be regarded as a colloidal system with unique mechanical properties. MBs are able to resonate in the ultrasound frequency range,[1,2] making them a powerful injectable contrast agent for ultrasound imaging.[3,4] Recently, MBs have been considered a potential multifunctional platform supporting therapeutics and diagnostics with the capability to target specifically pathological tissues and cells.[5] The structural element characterizing the overall behavior and properties of MBs is the shell confining the gas core from the dispersing medium which can be made of proteins, lipids, or polymers.[6] The shell of a lipid MB is a spherical surfactant monolayer, with a thickness of few nanometers, stabilized by weak interactions. Differently from lipid MBs, a layer of cross-linked polymer chains with varying extent of water permeation results in MBs having a shell thickness of some hundreds of nanometers.[7−9] Surprisingly, in some cases, the difference in shell thickness does not cause a huge change of the acoustic properties of the two types of MBs.[10] Lipid MBs are much easier to drive up to inertial cavitation by ultrasound (US) irradiation and have much shorter lifetime than polymer shelled MBs, reflected also in a dramatic shortening of the circulation life in a hostile environment for exogenous particles such as blood.[11−16] Moreover, lipid shelled MBs are less prone

Special Issue: Microbubbles: Exploring Gas-Liquid Interfaces for Biomedical Applications

Received: April 19, 2019
Revised: April 30, 2019
Published: May 1, 2019

DOI: 10.1021/acs.langmuir.9b01160
Langmuir 2019, 35, 10116−10127

for conjugating moieties enabling the active targeting or drug delivery because of the delicate packing at the basis of the surfactant shell layer.[17] Recently, phase change nanodroplets (NDs) stabilized by lipid, polymeric, or surfactant-based shells have been regarded as another way to obtain MBs by *in situ* US activation. This process, known as acoustic droplet vaporization (ADV), implies the transformation of NDs to MBs as final product and entails interesting features, which can be exploited in biomedicine:[18−21] (i) in the perfluorocarbon (PFC) core, hydrophobic drugs can be dispersed or solubilized;[22] (ii) phase change systems, subjected to ADV, have been also considered for the delivery of drugs previously loaded in the liquid core of the starting NDs;[23] (iii) the nanometric size of systemically administered droplets, is a remarkable feature in the presence of enhanced permeability and retention (EPR) effect, typically affecting tumor tissues, and can play a role in the penetration of biological barriers due to the vasculature leakiness.[24−28] Once the biological barrier is overcome after extravasation, the NDs engineered for active tumor targeting, can be converted into MBs by a US-triggered phase transition.[29] At this point MBs can be used both to support an enhanced ultrasound imaging and as therapeutic drug carrier and delivery device, bringing MBs to inertial cavitation and causing the local release of drug to the pathological tissue. From the literature it emerges that the energy threshold needed to trigger ADV is linked in a complex manner to the composition and structure of the NDs shell, its elasticity, and surface tension. Poly(lactic-glycolic) acid, PLGA, shelled NDs encapsulating perfluoropentane were used for carrying doxorubicin in the liquid core. A power of 8 W for 3 min was necessary for vaporizing the core of these NDs, a threshold much higher than the 3 W for few seconds used when the shell is lipidic.[30] Among lipid shelled NDs, we report here on a particular type which combines the features of the lipid ones with the robustness of a cross-linked structure. Park et al. reported on the incorporation of photopolymerizable diacetylenes into the formulation of phospholipidic MBs as a mean to accomplish tunable shell polymerization and enhanced stability of the microbubbles.[31] With this scenario in mind, we designed novel submicron-size, phase-change NDs to obtain MBs exhibiting features of both the lipid and the polymer MBs together. The shell encapsulating low boiling point PFCs, i.e. perfluoropentane (PFP) and perfluorobutane (PFB) with boiling points of 29 and −2 °C, respectively, is formed by a fatty acid monolayer consisting in 10,12-pentacosadiynoic acid (PCDA). A PCDA molecule exhibits interesting surfactant features with a carboxyl group as polar head and an aliphatic tail bearing two alkyne groups in positions 10 and 12, respectively. The diacetylene moiety during UV curing is subjected to an intermolecular topo-tactic free radical photopolymerization, yielding an alternate sequence of double and triple conjugated bonds transverse to the PCDA tails and connecting several single PCDA molecules, i.e. a poly(PCDA); the conjugation is evidenced by the appearance of a blue color. The result of the photopolymerization is a nanodroplet encapsulating a liquid PFC with a shell being intermediate between a lipid and a polymeric one (see Scheme 1) and exhibiting interesting optical properties already reported in the literature for UV cured PCDA films.[32−34]

Our investigation concerns the stability and the structure of the PCDA shelled nanodroplets after UV curing, the responsiveness to US irradiation, and ADV efficiency. We

Scheme 1. 1-4 Addition Polymerization of PCDA during UV Curing

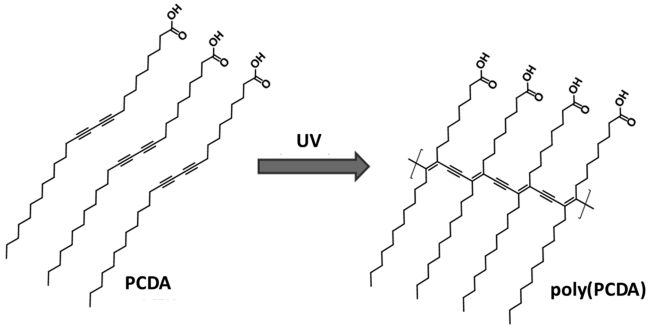

used poly(PCDA) shelled NDs with unusual stability and chemical versatility of the surface, for lipid NDs, as proof of concept to show new specific cells recognition ability and labeling of fluorescence probes. In this respect, the presence of functional diacetylenic and carboxylic moieties on one single PCDA molecule is functional to obtain a great variety of engineered phase shift hybrid devices incorporating near-infrared (NIR) absorbing nanomaterials.[35−40]

2. EXPERIMENTAL SECTION

2.1. Materials. The following materials were purchased from Sigma-Aldrich (Milan, Italy) and used without further purification: 10,12-pentacosadiynoic acid (PCDA), poly(ethylene glycol) 2-aminoethyl ether acetic acid (3000) (amino-PEG-COOH), pluronic F127, fluorescinamine isomer I, 1-ethyl-3-(3-(dimethylamino)propyl) carbodiimide hydrochloride (EDC), *N*-hydroxy-succinimide (NHS), 2-morpholinoethanesulfonic acid buffer (MES), acetic acid, 1,8,9-anthracenetriol (Dithranol), sodium chloride (NaCl), thiazolyl blue tetrazolium bromide (MTT), Dulbecco's modified Eagle's medium (DMEM), fetal bovine serum (FBS), L-glutamine, penicillin/streptomycin, and human serum. Perfluoropentane (PFP) and perfluobutane (PFB) were purchased from Apollo Scientific, UK; Irgacure 2959 and chloroform were purchased from BASF (Milan, Italy) and Alfa Aesar, respectively. Cyclo(Arg-Gly-Asp-D-Phe-Lys) (cRGD) was purchased from Avanti Polar (Milan, Italy). Methanol (MeOH) and dimethyl sulfoxide (DMSO) were purchased from Carlo Erba, Milan, Italy. Milli-Q (mQ) quality water (18.2 MΩ·cm) was produced by a Pure Lab deionization apparatus from USF (Perugia, Italy). Murine fibroblast cell line, NIH 3T3, was purchased from Istituto Zooprofilattico della Lombardia e dell'Emilia Romagna (Milan, Italy).

2.2. Methods. *2.2.1. Poly(PCDA)/PFC ND Formulation.* First, a 1 mM aqueous suspension of PCDA monomeric vesicles is prepared (see the Supporting Information). Then PCDA/PFP droplets were prepared by adding 50 μL of liquid PFP to 1 mL of PCDA monomer aqueous suspension cooled at 4 °C. The mixture is sonicated using a sonication bath cleaner (Ceia CP104, Florence, Italy) at full power for about 10 min (two iterations of 5 min each), until all PFP is incorporated into PCDA, leading to a milky solution. Then 10 μL of Pluronic F127 aqueous solution (10 mg/mL) is added as a stabilizer prior to polymerization. The droplets are immersed in an ice bath and photopolymerized under 365 nm UV light for 15 min using a UV lamp (7 W/cm^2) in the presence of Irgacure 2959 photoiniator (0.15% w/v). The development of a blue color in the suspension is taken as the visual evidence that the cross-linking reaction occurred. The UV cured droplets are washed with mQ water by centrifugation at 5200 rpm (2358 g-force) for 4 min.

As for PCDA/PFB droplets, first an empty vial sealed with a rubber septum is immersed in liquid nitrogen, then PFB gas is fluxed for few seconds inside the vial. As soon as the gas is liquefied, the vial is removed from the liquid nitrogen. Quickly 1 mL of PCDA aqueous suspension (1 mM) is added with a syringe and the mixture is

DOI: 10.1021/acs.langmuir.9b01160
Langmuir 2019, 35, 10116−10127

immediately placed in a sonication bath for 10 min at RT until obtaining a milky suspension. A fraction of PFB in the liquid state is incorporated by the PCDA molecules, while the remaining PFB evaporates in the empty volume of the vial, creating a pressure head over the liquid suspension. The droplets are subsequently UV cured for 15 min under 365 nm light, in the presence of Pluronic F127 and Irgacure 2959 at concentrations of 0.01% and 0.15% (w/v), respectively.

Both poly(PCDA)/PFP and poly(PCDA)/PFB samples were stored at 4 °C for further analysis and stability study.

2.2.2. PCDA Molecular Shell Density Determination. An estimate of the surface density number of surfactant molecules in the shell of poly(PCDA)/PFP NDs is carried out on a sample fraction with dimensions above 800 nm. Typically, 5 mL of poly(PCDA)/PFP were prepared as described previously and the largest NDs fraction was separated by centrifugation (2000 rpm, 360 g-force, 5 min). This fraction can be easily detectable and countable in a Neubauer chamber by bright field microscopy (40×). After elution in a column packed with Amberlite IR-120, (Merck, GE) proton exchange resin, the carboxyl groups of the PCDA shell in the selected fraction are titrated potentiometrically with a glass combined pH semimicroelectrode, (Crison, SP). Further details of this procedure are provided in the Supporting Information experimental section S2.

2.2.3. Chromatic Transition Study of poly(PCDA) Droplets. The chromatic transition of poly(PCDA) NDs upon heating is followed with an UV−vis double beam JASCO V-630 (Milan, Italy) UV−vis spectrophotometer with a 1 cm quartz cell (Hellma, GE) equipped with a Peltier unit (Jasco EHC-716, Milan, Italy), between 25 and 80 °C. The measurements were recorded taking water as reference and subtracting the spectra of PCDA NDs, before UV curing, to remove the scattering.

2.2.4. Dynamic Light Scattering (DLS). The size distribution of poly(PCDA)/PFC NDs is determined by DLS. A 1 mL portion of a 100 fold diluted solution of PFC encapsulated poly(PCDA) NDs is filled into a cylindrical quartz cuvette. The measurements are carried out at 90° using a photometer equipped with a BI-200SM goniometer, a BI-9000AT (Brookhaven Instruments Co.) correlation board and a solid state laser source emitting at 532 nm. Analysis of the autocorrelation function, g_2 (q, t), of the scattered intensity was carried out using the cumulants algorithm provided as part of the standard software package of the instrument.

2.2.5. Z-Potential. The Z potential of "blue" and "red" NDs (see section 2.2.2) suspended in mQ water is measured at 25.0 ± 0.1 °C with or without Pluronic F127 at a concentration of 0.1 mg/mL, used in the PCDA polymerization. A Phase Analysis Light Scattering (PALS) technique with a Malvern Nano ZetaSizer apparatus (Malvern Instruments Ltd., UK) equipped with palladium electrode dip cell ZEN 1002 (Malvern, UK) has been used for the measurement of the electrophoretic mobility and the related Z potential, provided herein in the Helmholtz−Smoluchowski approximation.[41]

2.2.6. Gel Permeation Chromatography (GPC). 2.2.6.1. Sample Preparation. A 12 mL portion of freshly generated poly(PCDA)/PFC NDs is freeze-dried, and the resulting powder is suspended just before measurement in DMSO containing 0.1% (w/v) lithium chloride, yielding a final concentration of 2 mg/mL.

2.2.6.2. Measurement. GPC analysis of polymerized NDs is performed using a Shimadzu instrument consisting of a controller unit (CBM-20A), a pumping unit (LC 20AT) equipped with a 20 μL sample loop, a degasser unit (DGU-20A3), a column oven (CTO-20AC), a diode array detector (SPD-M20A), and a refractive index detector (RID-10A); a Shimadzu Lab Solution software package (Version 5.42 SP3) allowed for the system control. APLgel 5 μm Mini MIX-C column (Agilent, 250 × 4.6 mm) eluted at 70 °C with DMSO containing 0.1% (m/v) lithium chloride was used, with a run-time of 20 min at 0.25 mL min^{-1} flow rate.

Molecular weights are calculated from a linear calibration (R^2 = 0.999) based on poly(styrene sulfonic acid) polymer fractions ranging from 4.3 to 2600 kDa using a dedicated excel-file reported previously.[42]

2.2.7. Matrix-Assisted Laser Desorption/Ionization−Time of Flight (MALDI-ToF) Mass Analysis. 2.2.7.1. Sample Preparation. One mL of freshly generated poly(PCDA)/PFC NDs is centrifuged at 3900 rpm (1326 g-force) for 4 min, and the recovered pellet is suspended in aqueous buffer solutions, i.e., acetate buffer (0.1 M, pH 4.5) or phosphate buffer (0.1 M, pH 8) at a final concentration of 4 mg/mL. The buffer suspensions of NDs are mixed (1:1 v/v) with a matrix solution of dithranol at 2 mg/mL in NaCl aqueous solution (10 mg/mL) just before measurement. A 2 μL portion of the resulting analysis solution is placed on the MALDI-TOF sample holder and left for drying in the dark.

2.2.7.2. Measurement. Measurements are performed on a Voyager-DE PRO Biospectrometry Workstation MALDI-TOF mass spectrometer by Applied Biosystems (USA), equipped with a nitrogen laser (337 nm) using the Applied Biosystems operating and analysis software, monitoring a mass range between 200−5000 Da in positive linear mode. The delayed extraction technique is used applying delay times of 200 ns. An accelerating voltage of 25.0 kV, a laser intensity of around 2000 eV, a grid voltage of 95%, and a guide wire voltage rate of 0.2% were used for generation of optimum spectra. Spectra were collected in positive and negative mode, adjusting laser intensity as necessary. Analyzed spectra are the sum of 50 to 250 shots. The instrument was calibrated using commercially available PEG standards in the range between 500 and 10 000 Da.

Mass analysis and spectra interpretation was achieved using Applied Biosystems Data Explorer and a combinatorial excel-based analysis.

2.2.8. Bright Field, Transmission, and CLSM Microscopies. Although close to instrumental resolution, an overall view of the different droplet samples is carried out using an inverted Eclipse model Ti-E microscope (Nikon Instruments, Japan) equipped with a 40× long-working distance objective, a 60×/1.4 oil immersion Plan Apo objective, an Ar^+ green laser (λ_{exc} = 488 nm) (Melles Griot, Carlsbad, CA), and a He−Ne laser (λ_{exc} = 543 nm) (Spectra Physics, Mountain View, CA). An estimation of the poly(PCDA)/PFC droplets concentrations is assessed by bright field microscopy using a Nauber chamber 0.25 μm × 0.25 μm × 0.1 μm and imageJ software (freeware) to analyze micrographs. ADV is monitored by fluorescence and confocal microscopy for fluoresceinamine conjugated PCDA/PFP droplets (λ exc 488 nm).

2.2.9. Acoustic Droplet Vaporization (ADV). The ADV experiments are performed using a SP100 sonoporator (1 MHz) from SONIDEL (Dublin, IE). Typically, for each polymerized droplets systems described above, an "Ibidi" channel slide 50 mm × 5 mm × 0.4 mm (Milan, Italy) is filled with 200 μL of 10-fold diluted droplets suspension and fixed in a polystyrene flask degassed water bath placed on the microscope. An ultrasound probe is placed in the water bath at 37 °C and at 2 cm height. Acoustic vaporization is carried out at 1 MHz central frequency, 100% duty cycle for 30 s and at different US powers to assess the efficiency of each type of PFC filled poly(PCDA) droplets. The transition NDs → MBs is followed by bright field microscopy. For these experiments droplets in the channel were diluted in human serum.

2.2.10. Acoustic Attenuation Measurements. The experimental setup is described in Scheme S1 in the Supporting Information. Typically, a glass cell (2 cm × 2 cm × 4 cm) is filled with aqueous droplet suspensions in degassed DMEM (at an estimated concentration of 3 × 10^7 NDs/mL). The latter features two openings at opposite sides separated by a distance of 2 cm allowing contact with the emitting and receiving transducers. Two flat 10 MHz transducers (Olympus V311) as emitter and receiver and a waveform generator producing consecutive sinusoidal ultrasound bursts at frequencies ranging from 0.5 to 20 MHz (in steps of 0.25 MHz) are used. A constant input voltage of 6 V was applied at each frequency, resulting in acoustic pressure levels below 60 kPa. The attenuation was deduced from the transmitted signals detected by the receiver by means of a reference method, where the reference is the DMEM medium. Acoustic attenuation measurements of poly(PCDA)/PFP and poly(PCDA)/PFB NDs are performed before and after ADV. For the ADV attenuation measurements, the sonoporator head is carefully

DOI: 10.1021/acs.langmuir.9b01160
Langmuir 2019, 35, 10116−10127

immersed on the top of the cell, and the droplets are irradiated with the same parameters described in the ADV section above (duty cycle 100, 0.1−3.6 W/cm^2, 30 s).

2.2.11. MTT Cytotoxicity Evaluation of poly(PCDA)PFP Droplets. For MTT assays, typically, 5×10^4 of fibroblasts NIH 3T3 are seeded in 24-well plates and cultured in DMEM supplemented with 2 mM L-glutamine, 1% penicillin/streptomycin, and 10% FBS at 37 °C in a humidified atmosphere containing 5% CO_2. The multiwell plates containing the cells were left for 12 h in incubator (HeraCell 150i, Thermo-Scientific) to allow cell adhesion. Afterward, 900 μL of DMEM and 100 μL corresponding to amounts ranging from about 10^5 to 5×10^8 (droplets/mL) of poly(PCDA)/PFP droplets were added. After 24 h contact, the cells are washed twice with PBS and incubated for 4 h with MTT at a final concentration of 0.5 mg/mL in serum-free DMEM, at 37 °C under 5% CO_2. Then, MTT is removed and the water-insoluble formazan crystals formed as byproduct of the test are dissolved in DMSO. Spectrophotometer absorbance measurements at 570 and 650 nm wavelengths were carried out. The cell viability is expressed according to eq 1 as percentage value representing mitochondrial activity. Untreated cells (NT), i.e. without being in contact with the droplets, are used as control.

$$\text{cell viability (\%)} = \frac{(\text{AbsNDs})_{570} - (\text{AbsNDs})_{650}}{(\text{AbsNT})_{570} - (\text{AbsNT})_{650}} \times 100 \quad (1)$$

where Abs is the absorbance and NDs represents a poly(PCDA)/PFP droplets treated cells. Data were statistically analyzed using the paired Student *t* test within the groups.[43]

2.2.12. Functionalization of poly(PCDA)/PFP NDs. 2.2.12.1. Poly-(PCDA)/PFP Fluoresceinamine Labeled Droplets. Fluoresceinamine dye is conjugated to the poly(PCDA)/PFP (blue) submicron droplets by EDC/NHS chemistry through the carboxylic moiety of the PCDA monolayer at the PFP/water interface and the $-NH_2$ group of the fluorescent label (see Scheme S3 in the Supporting Information). Typically, the carboxylic groups of the polymerized droplets, prepared as described in section 2.2.1, are activated with an equimolar amount of EDC/NHS (approximately 2 μmol) at pH fixed to 6.5 with MES buffer (0.1 M). The suspension is kept under stirring in the dark at RT for 30 min. Then 2 μmol of dye solution in MeOH/H_2O (1:1 v/v) are added and the suspension is further kept under stirring for 2 h. Finally the covalently labeled droplets are washed with mQ water by a multistep centrifugation at 5200 rpm (2358 g-force) for 4 min to remove unbound dye.

2.2.12.2. RGD-Functionalized PCDA/PFC Droplets for in Vitro Cell Targeting. Preparation. The strategy for the tagging of poly(PCDA) NDs with *c*RGD peptide consists in a double EDC/NHS chemistry. In a first step, a PEG chain bearing NH_2 and COOH as end groups is tethered on the shell of the NDs via EDC/NHS leading to an amide bond through the primary amine group of PEG and the carboxyl groups on the NDs surface. Typically 1 μmol of NDs is suspended in a MES buffer (0.1 M, pH 6.5) and activated by EDC/NHS (2 μmol) for 30 min following the addition of 2 μmol of amino-PEG-COOH. The reaction is carried out for 2 h at RT under gentle stirring. Then NDs are washed with MES buffer to eliminate unbound PEG chains by centrifugation (5000 rpm/2180 g-force). In a second step, the resulting droplets are activated by 0.5 μmol EDC/NHS for 30 min following the addition of cRGD bearing a D-Phe-Lys moiety (0.5 μmol). Thereafter, the functionalized cRGD NDs (poly(PCDA)-PEG-cRGD/PFP) are washed by centrifugation (5000 rpm/2180 g-force, 4 min) and heated at 70 °C to pass from the blue to the red form, with a partial decrease of the average dimensions. This step is necessary in order to attribute fluorescence to the NDs for an easy detection in the adhesion tests, which avoids a further labeling step of NDs.

In vitro cell targeting. HUVEC cells were cultured in DMEM supplemented with 2 mM L-glutamine, 10% FBS, and 1% penicillin/streptomycin at 37 °C in a humidified atmosphere containing 5% CO_2. In a typical flow experiment, flow chamber slides (μ-Slides I 0.4) are coated with 2% gelatin solution according to the Ibidi protocol, after which 10^5 of HUVEC cells are seeded. To allow cells to grow and adhere on the bottom of the chamber slides, μ-Slides I 0.4 were put in the incubator (HeraCell 150i, Thermo Fisher Scientific) and left overnight. Afterward, cells are washed three times with PBS/FBS/DMEM (40%, 40%, 10%) (v/v) and placed under an inverted microscope (Nikon Inverted Microscope Eclipse Ti-E) equipped with a 40× objective (Nikon, Japan), a motorized stage, and the Zylas CMOS camera 4.2 (Andor, Belfast, UK). The setup, assembled as described in Scheme 2, consists of an infusion pump with a 10 mL

Scheme 2. *In Vitro* Cell Targeting Setup

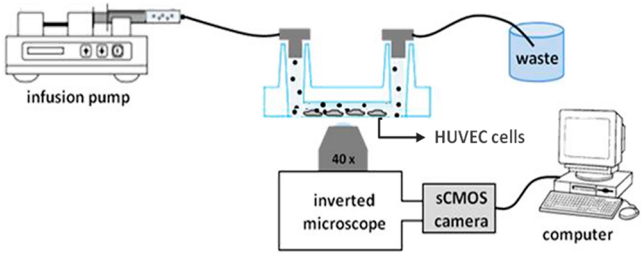

syringe filled with the NDs (0.1 mM) suspension in the PBS/FBS/DMEM mixture and connected by silicon tubing (20 cm, internal diameter 1.6 mm, and outer diameter 3.2 mm) and Luer-lock connector adapters to the μ-Slide. HUVEC cells were grown at confluence on the bottom side of the channel slide. The poly(PCDA)-PEG/PFP and poly(PCDA)PEG-*c*RGD/PFP NDs, suspended in cell medium containing FBS, were fluxed for 10 min at a shear stress corresponding to 1 dyn/cm^2 (flow rate 1.12 mL/min) allowing for interaction with cells.

The channel slide is then upside down inverted for 5 min, then placed under the microscope, and fluxed for 10 min with PBS to wash out any unspecifically adhered and easily detachable NDs. To image the NDs in fluorescence microscopy we took advantage of the intrinsic fluorescence of the NDs after conversion into the red form (λ_{ex} 543 nm). Pictures corresponding to the five different fields of view are recorded after the washing. For image capturing and data analysis, Nikon NIS-Element AR software is used.

3. RESULTS AND DISCUSSION

3.1. Poly(PCDA)/PFC Droplet Formulation Mechanism. PCDA monomers can form vesicles with a bilayer arrangement in aqueous solutions with the polar heads oriented toward the water interface.[44−48] In the case of PFC NDs, possible shell forming self-assembly of the PCDA units can result in a monolayer, triple layer or more, as described in Scheme S2 of the Supporting Information. Counting NDs with an average diameter larger than 800 nm, detectable by bright field microscopy, the average surface occupied per PCDA molecules, i.e. 45 Å^2, was determined by titrating the carboxyl moiety of the NDs shells (see Figure S1 of the Supporting Information). Considering the curvature of the ND surface, this value is in line with the reported value, 26 Å^2, for Langmuir−Blodgett (LB) films of PCDA.[49] An overcompression of an LB monolayer film by applying a surface pressure of 20 mM/m causes a film reorganization into a triple layer one with a molecular area of 7 Å^2.[50] Therefore, the molecular area of UV cured NDs measured in this work, although affected by a large error, up to 30%, essentially due to the counting procedure, suggests that the PCDA shell of NDs is a monolayer analogous to LB film assembly.

Thus, the PCDA monolayer shells encapsulating a PFC liquid core in aqueous medium, are oriented with the lipophilic tail toward PFC, whereas the hydrophilic carboxylic head points toward the aqueous phase (see Scheme 3). PCDA shells

DOI: 10.1021/acs.langmuir.9b01160
Langmuir 2019, 35, 10116−10127

Scheme 3. Poly(PCDA)/PFP Nanodroplet Formulation and Chromatism

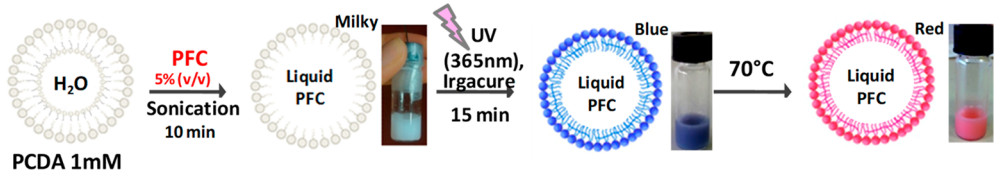

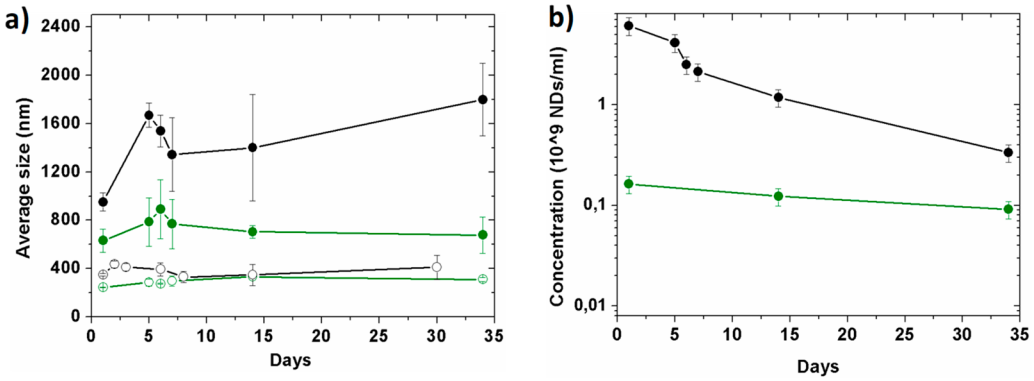

Figure 1. (a) Average size variation of poly(PCDA)/PFP (black) and poly(PCDA)/PFB (green) over time by DLS. The filled and empty symbols represent NDs with initially larger and smaller size, respectively. (b) Poly(PCDA)/PFP (black) and poly(PCDA)/PFB (green) concentration over time (the lines represent guides for the eyes). Fractions of NDs with selected dimensions are obtained by separating pellet and supernatant, respectively, upon centrifugation at 3200 rpm/973 g-force for 4 min.

can encapsulate different PFC already available on the market and, among them, some are FDA approved. PFC boiling points are found in a wide temperature range, depending on the carbon chain length and the fluorine/hydrogen ratio. Accordingly, PFCs can be liquid or gas in standard conditions, i.e. 1 atm. A milky PCDA/PFP droplets dispersion can be easily formed by sonicating a mixture of PCDA aqueous suspension and liquid PFP. However, to obtain stable droplets with PFB (bp = −2 °C), the latter needs to be liquefied under pressure or at very low temperatures. Sheeran et al. showed an interesting route to obtain PFB encapsulated droplets by condensing commercially available microbubbles, known as Micro-Marker (VisualSonics, Canada). This was achieved by cooling the MBs and applying a pressure of 170 kPa.[51] Therefore, PFB NDs can be directly obtained once PFB is liquefied at low temperature, under pressure, or both. In our case, the PFB was brought to liquid nitrogen temperature in order to limit the evaporation during further manipulations carried out at room temperature in a closed vessel, as described in the Experimental Section. Additionally, the Laplace pressure contributes in stabilizing the nanodroplets by increasing the boiling temperature of PFB liquid core. Using the PFB Antoine's parameters,[52] a boiling temperature of about 60 °C is obtained when the external pressure is 3.4 atm, corresponding to the vapor pressure of PFB at room temperature. This explains also why the majority of the NDs encapsulating PFB have diameter values around 250 nm. Those with larger diameters, i.e. having less surface curvature, are less stable, and most of them are bound to burst.

The photopolymerization of PCDA increases the stability of the formed NDs. During UV curing on the shell of the NDs, the hydrophobic tails of the PCDA molecules bearing diacetylene moieties are subjected to free radical polymerization. Strict PCDA molecular orientation is required to accomplish a topo-tactic sequence of alternating ene-yne bonds connecting transversally several PCDA tails, forming polymerized PCDA species of different lengths and molecular weights in the shell. The aqueous suspension of polymerized poly(PCDA)/PFC NDs is characterized by an intense blue color due to the conjugation of the double−triple bonds alternating sequences, whose intensity depends on the irradiation time and therefore on the polymerization degree. Moreover, the "blue" species can undergo a chromatic transition to a fluorescent red color upon heating,[28] as illustrated in Scheme 3 and Figures S2 and S3 of the Supporting Information.

3.2. Stability of poly(PCDA)/PFP and poly(PCDA)/PFB Droplets. Both PFP and PFB poly(PCDA) shelled droplets exhibit a large size distribution in the submicron range of 200−1000 nm, which can be tuned by centrifugation (see Figure S4 and Table S1 in the Supporting Information). However, for the PFB based droplets, in agreement with the findings reported by Sheeran et al., only those with a size below 500 nm remain stable once subjected to atmospheric pressure and RT.[53] Average sizes of PFB and PFP encapsulating NDs, are monitored by DLS and reported as a function of time in Figure 1a. Sizes below 600 nm for both PFP and PFB NDs stay constant for more than a month, while the larger sizes in the case of PFP NDs increase by a factor of 2 within the first 5 days. NDs counts, estimated by optical microscopy over the same period of time, show as indicated in Figure 1b a pronounced decrease for poly(PCDA)/PFP of the NDs number, occurring again in the first 5 days. The time evolution of the NDs highlights a good NDs stability over a month, with a size increase and a numerical concentration drop occurring in the first 5 days. The lower stability of NDs with an initial larger size could be explained by a limited polymerization of PCDA, due to the larger distance separating the PCDA molecules as consequence of a lower density of monomers over the larger PFP core.

Moreover poly(PCDA)/PFC samples exhibit strong negative Z-potential, stabilizing the colloidal system, with no

DOI: 10.1021/acs.langmuir.9b01160
Langmuir 2019, 35, 10116−10127

significant difference for both blue and red forms (−32 ± 2 and −33 ± 2 mV, respectively). Therefore, the heat treatment maintains the ionization of the carboxyl moiety at the poly(PCDA) shell surface unchanged, suggesting that the chromatic transition is attributed to minor structural variations limited to the orientation of the carboxyl groups.

3.3. Poly(PCDA)/PFC ND Shell Characterization by GPC and MALDI-ToF. The degree of polymerization of the shell of poly(PCDA)/PFC NDs is investigated by GPC and MALDI-ToF for samples treated with different UV curing times. Figure 2 shows the MW distributions obtained for

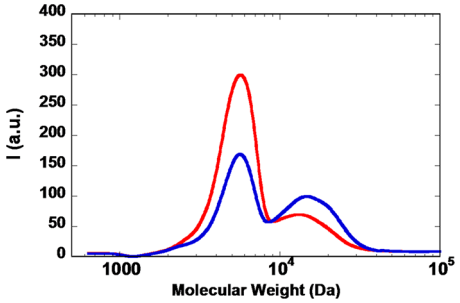

Figure 2. Molecular weight distribution of freeze-dried NDs polymerized for 5 min (red) and for 15 min (blue). Chromatograms were normalized to the area of the peaks.

poly(PCDA) shells with UV curing of 5 and 15 min, respectively, in comparison to the PCDA monomer. The chromatograms display a higher peak at around 5800 Da and a lower peak at 15500 Da corresponding to a polymerization degree of 16 and 41, respectively.

The UV curing time has a deep influence on the chromatogram shapes, changing the relative heights of the two peaks. The intensity of the peak of the low molecular weight species decreases when the curing time changes from 5 to 15 min, whereas the opposite behavior is observed for the high molecular weight peak. Moreover, a shoulder is observed at around 20 000 Da, highlighting the presence of higher molecular weight species. These findings confirm that the UV triggered radical polymerization is responsible for the polymerization of PCDA and that the time frame characteristic of this reaction covers several minutes. MALDI-ToF based mass analyses confirm the GPC results. Spectra are recorded after redispersing poly(PCDA)/PFC samples in acetate buffer (positive mode) and in phosphate buffer (negative mode). Combinatorial analysis performed to quantify the primary MALDI-ToF MW-distributions indicates molecular weights as high as those found by the GPC analysis as described Figures 3 and S5 (Supporting Information).

Based on the chemical nature of the poly(PCDA) chains investigated in this study, a multiple charging process is likely to occur in acetate buffer by multiple addition of protons and sodium cations or, in phosphate buffer, by multiple deprotonation combined with a partial charge compensation by proton and sodium addition, which should explain the low mass/charge values reported in Figures 3 and S5. Moreover, it can be assumed that the rather hydrophobic nature of the poly(PCDA) chains allowed for observation of poly(PCDA)-dithranol complexes. Significant results of the combinatorial analyses are summarized in Tables S2 and S3 of the Supporting Information for negative and positive mode, respectively. In this analysis, also the mentioned possible stacking complexes

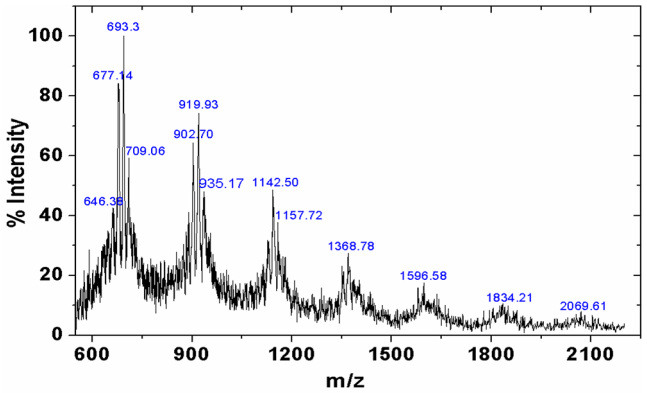

Figure 3. Representative MALDI-ToF spectrum obtained in negative mode for poly(PCDA)/PFC NDs polymerized under UV irradiation for 15 min dispersed in phosphate buffer in the presence of dithranol as a matrix reagent.

between the poly(PCDA) and the matrix molecules have been considered. Structural representations of selected identified polydiacetylene species are illustrated in Scheme S4 of the Supporting Information. Such analysis suggests that high degrees of polymerization are obtained when polymerizing PCDA by UV curing. The identified polymer sizes fit in the bulk of the chromatogram of Figure 2, confirming a bimodal distribution of the poly(PCDA) molecular weights with a prevailing peak at around 8000 Da (DP = 22) and a minor peak at about 15 000 Da (DP = 39). According to our GPC and MALDI-ToF results, about 40 PCDA molecules have been polymerized by UV curing organized in patches of surfactant cross-linked molecules with a 2D size of about 200 nm^2.

3.4. Acoustic Droplet Vaporization (ADV) of poly-(PCDA)/PFC. ADV experiments are carried out *in vitro* at 37 °C, with nanodroplets dispersed in human serum in order to mimic as much as possible the physiological conditions. Indeed, the presence of proteins in blood serum such as albumin lowers the surface tension of droplets and therefore impacts favorably on the ADV efficiency by rendering the process more efficient. Droplets of encapsulated PFP or PFB required different conditions to achieve ADV, according to their different boiling points. In our tests, US intensities of 3.6 and 0.5 W/cm^2 are applied on the PFP and PFB NDs, respectively. The most direct evidence supporting the occurrence of the liquid ↔ vapor transition of the core is the observation of an abrupt change of size of the insonified NDs, passing from submicron to MBs with diameters of few microns. Micrographs in Figure 4a and c show that, before US activation, both PFP and PFB NDs are hardly detectable in bright field modality, as their size is below or at the most approaching the resolution limit of the microscope.

Moreover, in the same region of interest, ROI, or in different zones of the channel micron-sized particles, i.e. MBs, were not visualized. This finding confirms the stability of the NDs and rules out the hypothesis of a spontaneous phase transition process slowly progressing during the observation. After US irradiation a relevant number of MBs appears (see Figures 4b and d). The size of the ADV generated MBs does not exceed 10 μm in size as required for a systemically injectable device. The average size of the MBs depends on the size of the parent NDs but also on the PFC core, as highlighted in Table 1. After ADV, the average size of poly(PCDA)/PFP NDs increased by

DOI: 10.1021/acs.langmuir.9b01160
Langmuir 2019, 35, 10116−10127

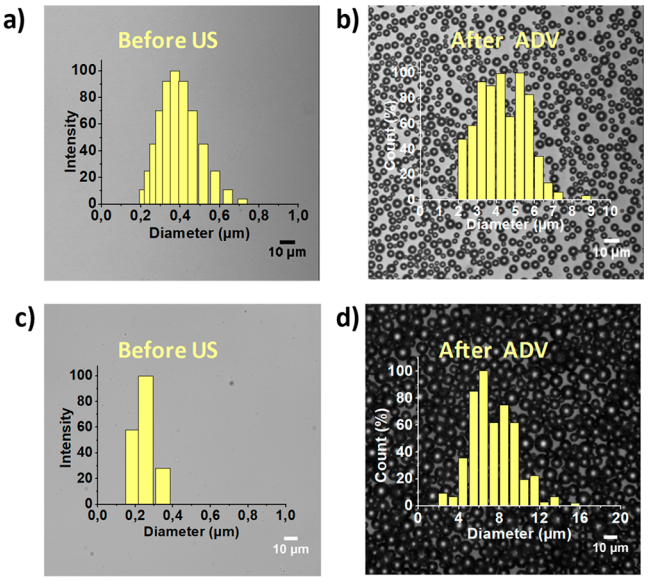

Figure 4. Poly(PCDA)/PFP nanodroplets before (a) and after (b) ADV at 3.6 W/cm^2, respectively; poly(PCDA)/PFB nanodroplets before (c) and after (d) ADV at 0.5 W/cm^2, respectively. Micrographs (b and d) were taken after 10 min from the US activation.

a factor of 10, whereas poly(PCDA)/PFB MBs displayed an average size 30-fold larger than the parent NDs.

Table 1. Poly(PCDA)/PFC Size before and after ADV

type	NDs diameter (nm) [before ADV]	MBs diameter (μm) [after ADV]
Poly(PCDA)/PF	400 ± 20	5 ± 1
	700 ± 120	8 ± 3
Poly(PCDA)/PFP "red"	760 ± 100	9.4 ± 2.7
Poly(PCDA)/PFB	250 ± 10	7.5 ± 2.7

It was reported that ADV promotes a size increase of about 5- to 6-fold over a millisecond time lapse for phospholipidic NDs, in agreement with simple considerations based on ideal gas.[45,46] However, MB size has a complex dependence, not yet completely elucidated,[47] on medium, perfluorocarbon characteristics, shell type.[47] Time is a factor to take into account in analyzing NDs ↔ MBs transition. Reznik et al. reported on 400 nm PFC encapsulating droplets which expand into MBs with a diameter of 1.4 μm after 1 ms and 5.6 μm after 1s from ADV.[54] Sheeran et al. have shown that there is a significant difference in the size increase between degassed and undegassed samples upon ADV, suggesting that undegassed samples tend to increase more in size over time,[48] excluding a coalescence effect between MBs. An increase of about 25 times of the particle diameter, after ADV, is reported for droplets of PFP stabilized in a suspension of saline containing bovine serum albumin. This further expansion was explained by accounting for an uptake of gases from the air-saturated host medium into the MBs.[55] These conditions apply also to our experiments, performed in undegassed medium containing human serum to mimic as much as possible the physiological conditions. Our results indicate that the behavior of the microbubbles after ADV depends on the boiling point of the liquid core of the parent nanodroplets. If the latter is superheated (as in the case of PFB), the microbubble lifetime could be surprisingly long. It has been reported that lipid coated microbubbles with a size range of 1−5 μm encapsulating air lasted for up to one year dispersed in degassed water.[56] Such prolonged lifetime was attributed to the surfactant coating of the MBs due to the shell resistance to gas permeation. In our systems the stability conditions are more favorable than in the reported example, due to the marked hydrophobicity of the encapsulated gas (more than the air), resulting in a very little tendency to diffuse out in an aqueous environment. No evidence of bursts or inertial cavitation, IC, in the form of broken shells or debris were observed after US irradiation. ADV proceeded without accompanying IC events, in agreement with studies reporting that the thresholds of these two processes are not governed by the same parameters nor have the same dependence from the US frequency of irradiation.[57] With liquid PFCs, boiling higher than 37 °C, not considered in this work, microbubbles revert to nanodroplets within few minutes, indicating that the hydrophobic gas core remains encapsulated in the poly(PCDA) shell during microbubbles' life. However, we cannot exclude that, with low boiling point perfluorocarbons, the occurrence of gas leaks from the shell could be a mechanism leading to a decrease of the number of microbubbles as we cannot detect a recovery to the nanodroplets state. The permeation of highly hydrophobic perfluorocarbons in the dispersing aqueous medium is discouraged, even for partially cross-linked poly(PCDA) shell, delaying the escape from the microbubbles.

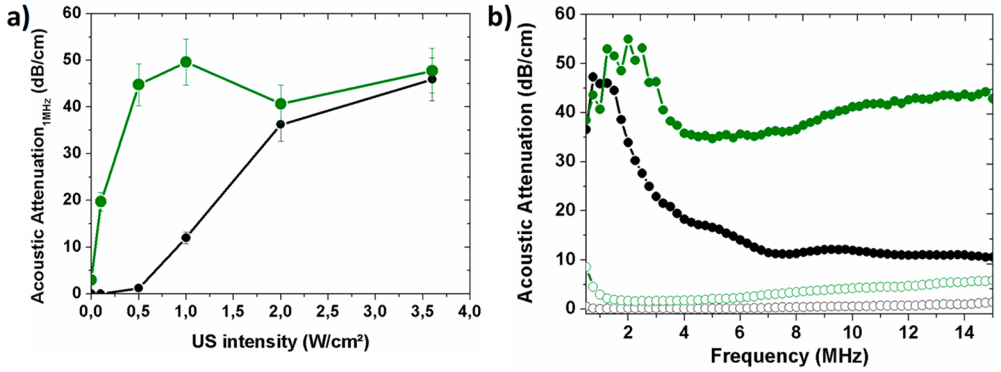

Figure 5. (a) Acoustic attenuation at 1 MHz as a function of applied US intensity for poly(PCDA)/PFP (black) and poly(PCDA)/PFB (green); (b) acoustic attenuation spectra of poly(PCDA)/PFP (black) and poly(PCDA)/PFB (green) nanodroplets before (empty markers) and after ADV (filled markers) at 3.6 and 0.5 W/cm^2, respectively (lines are a guide for the eyes).

DOI: 10.1021/acs.langmuir.9b01160
Langmuir 2019, 35, 10116−10127

3.5. Acoustic Attenuation of poly(PCDA)/PFC NDs. The acoustic attenuation measurements of nanodroplets before and after irradiation with US at 1 MHz were performed at 37 °C, in a degassed cell culture medium containing FBS. Figure 5a shows that the attenuation of PFP NDs measured at 1 MHz increases by increasing the intensity of the applied US up to 3.6 W/cm^2, whereas the poly(PCDA)/PFB NDs attenuation reaches a maximum when the power of the incident US irradiation is only 0.5 W/cm^2, consistently with the lower boiling point of PFB (−2 °C). The dramatic change of attenuation before and after US irradiation indicates that the process is a liquid−vapor transition and not an aggregation/coalescence effect where the absence of a phase transition could not justify such a remarkable attenuation increase. Moreover, the poly(PCDA)/PFP NDs do not exhibit any acoustic response before their activation, even at the physiological temperature of 37 °C. The behavior of the poly(PCDA)/PFB NDs, which show a very low, but detectable, acoustic attenuation (see Figure 5b), is attributed to a small fraction of larger PFB droplets with the core partially or already completely vaporized, although not detected in bright field microscopy. This is supported by the attenuation spectra of PFB encapsulated NDs without US activation as a function of the time. The results reported in Figure S6 of the Supporting Information show that attenuation is absent for NDs with small size (300 nm), suggesting that no spontaneous vaporization occurred. PFB NDs with larger size (700 nm as average) display vaporization as indicated by the low but not negligible attenuation recorded within 1 min. It is worth noticing that the attenuation spectra after ADV for both types of NDs, i.e., the PFP and PFB based poly(PCDA), reveal an acoustic resonance between 1 and 2 MHz similar to the peak resonance of lipid shelled MBs.[58−61]

3.6. Cytotoxicity Evaluation of poly(PCDA)/PFC Droplets. Many studies reported the use of PCDA for drug delivery applications in the form of liposomes or monolayer films for biosensing applications due to its optical features and sensitivity to external stimuli once polymerized.[32,62] Hybrid systems incorporating PCDA have been investigated for their cytotoxicity. However, as far as we know, no data are available concerning the impact of the poly(PCDA) combined with PFCs on living tissues. Studying the viability of NIH 3T3 fibroblasts after 24 h of incubation with different ND concentrations, we demonstrate the biocompatibility of poly(PCDA). The test is performed only on PFP based droplets since NDs encapsulating PFB do not allow viability tests at high concentrations at 37 °C for 24 h, due to their limited stability in these conditions. Figure 6 shows that, within the error of MTT tests, no significant decrease in cells viability occurs, when compared with the control even for the highest amount estimated as 5 × 10^8 droplets/mL.

3.7. Poly(PCDA)/PFP ND Surface Modifications. *3.7.1. Functionalization with Fluoresceinamine.* The presence of carboxyl groups as polar head exposed on the surface of PCDA/PFC NDs offers the possibility to tailor the chemistry at the water interface of the construct after UV curing and allows for easy surface modifications to implement their functionalities by attaching ligand molecules, small dyes, nanoparticles, etc.[63−65] Molecules with primary amine groups can be coupled to the carboxyl groups of PCDA NDs in aqueous media via zero length spacer EDC/NHS chemistry. As a proof of concept, the fluoresceinamine dye is conjugated to poly(PCDA)/PFP NDs for labeling the shell (see Scheme S3 in the Supporting Information). The resulting NDs appear as single fluorescent green pixels when excited with an Ar$^+$ laser at 488 nm. The shell modification did not hinder ADV for converting the NDs into MBs, as highlighted in Figure 7d. It can be noticed that the fluorescence emission decreases due to both the expansion of the shell and the corresponding decrease of the fluorophore density; visualization is nevertheless possible increasing the gain (see Figure 7).

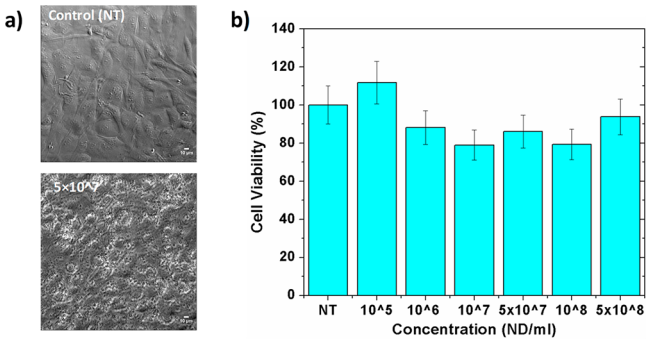

Figure 6. Cytotoxicity evaluation of poly(PCDA)/PFP droplets by MTT tests on fibroblasts NIH 3T3: (a) control cells (in the absence of poly(PCDA)/PFP NDs) and cells exposed to an indicative amount of 5 × 10^7 NDs; (b) cell viability histogram as a function of droplet concentration.

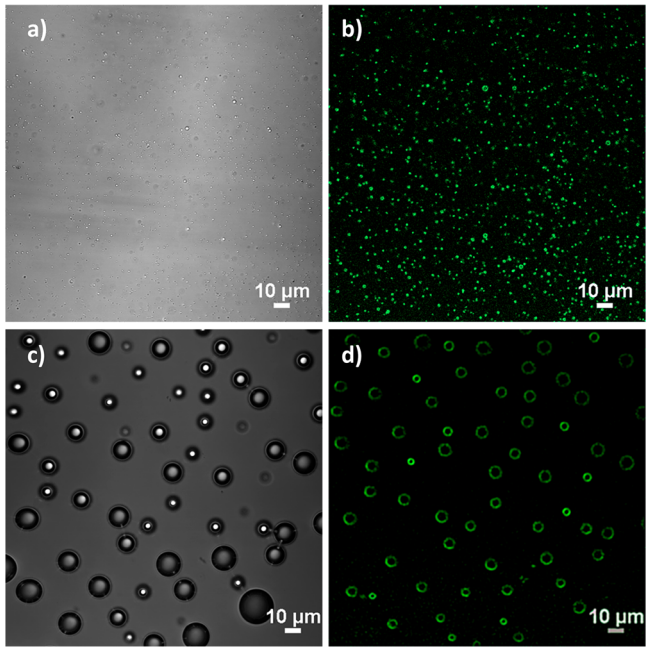

Figure 7. Poly(PCDA)/PFP-Fluoresceinamine before ADV: (a and b) transmission microscopy and confocal microscopies, respectively. After ADV: (c and d) transmission and confocal microscopies, respectively. In d, gain was increased from 145 to 150 (pinhole: small 30 μm).

3.7.2. Functionalization with Cyclo-RGD and in Vitro HUVEC Cell Targeting. Various peptides can provide specific interactions with cells and promote bioadhesion by recognition of specific receptors present on target sites. RGD is a sequence of arginine, glycine, and aspartic acid, commonly known for targeting $\alpha_v\beta_3$ integrins overexpressed in tumor cells during angiogenesis.[66−69] A pentapeptide, which includes the RGD sequence followed by a D-Phe-Lys moiety to close the cyclic

DOI: 10.1021/acs.langmuir.9b01160
Langmuir 2019, 35, 10116−10127

Scheme 4. PEGylation and Conjugation with cRGD Peptide of Poly(PCDA)/PFC NDs

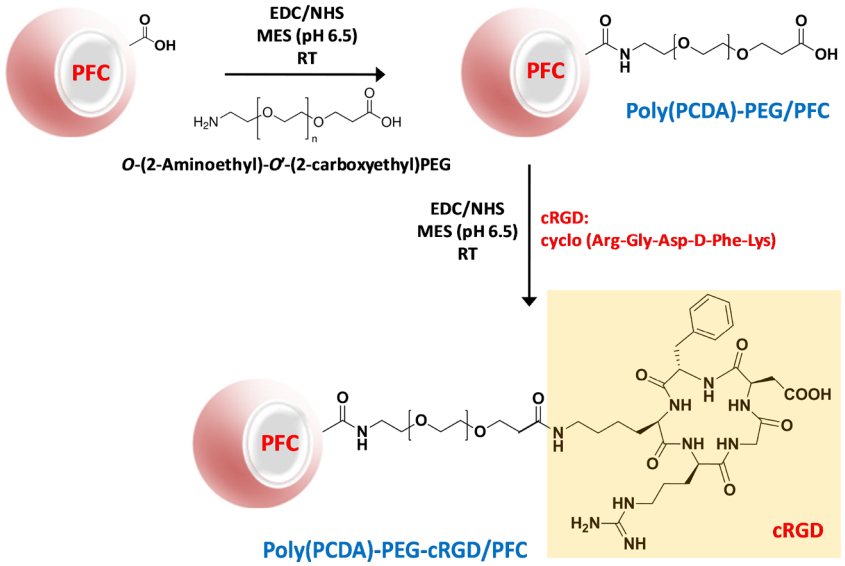

structure, i.e. cyclo (Arg-Gly-Asp-D-Phe-Lys) or cRGD, has been chosen in order to enable tethering onto the surface of the poly(PCDA) NDs via EDC/NHS chemistry, as described in Scheme 4. In this study we are focused on the biointerface properties of the NDs as this is the form designed to target and tether pathological cells. It should be considered that, *in vivo*, a factor which interferes with the tethering of NDs to cells is the buildup of a plasma protein corona on the NDs shell once the construct is injected in the blood pool.[66,70] We found a marked adhesion of NDs without cRGD functionalization on HUVECs. Another factor perturbing the efficacy of the active targeting of integrins rich cells is the high density of carboxyl groups on the NDs surface, which can promote a strong, although nonspecific, tendency to interact with cells. The presence of such additional interaction with cells masks and competes with the efficiency of the active cRGD promoted targeting of integrin receptors. In an effort to prevent or limit the establishment of a protein corona and the nonspecific targeting, cRGD has been tethered to the surface of the poly(PCDA) NDs via a PEG spacer to facilitate the spatial orientation of cRGD by the enhanced linker flexibility and to increase the distance of the cRGD from the NDs surface to avoid nonspecific interactions of the polar heads of PCDA with the cell membrane and to place the cRGD ligand molecules above any potential protein corona.

Figure 8 illustrates the bioadhesion study in dynamic conditions, i.e. steadily perfusing the suspension of targeted and PEGylated "red" form of poly(PCDA) NDs through microchannels in which HUVEC cells have been previously seeded and brought to confluence. Pegylation is an efficient method to limit the unspecific interactions of NDs with HUVEC cells, promoted by the presence on the shells of a large number of carboxyl groups.[71] NDs, converted into the red fluorescent form for immediate optical and fluorescence microscopy detection without the addition of any external fluorescence labels, appear as "red pixels" due to the ND dimensions below the microscope optical resolution. Comparison on the number of bioadhered pegylated NDs with and without RGD modification over the HUVEC cells cultured in the microchannel slide suggests an enhanced targeting specificity of RGD modified NDs surfaces. The channel slide

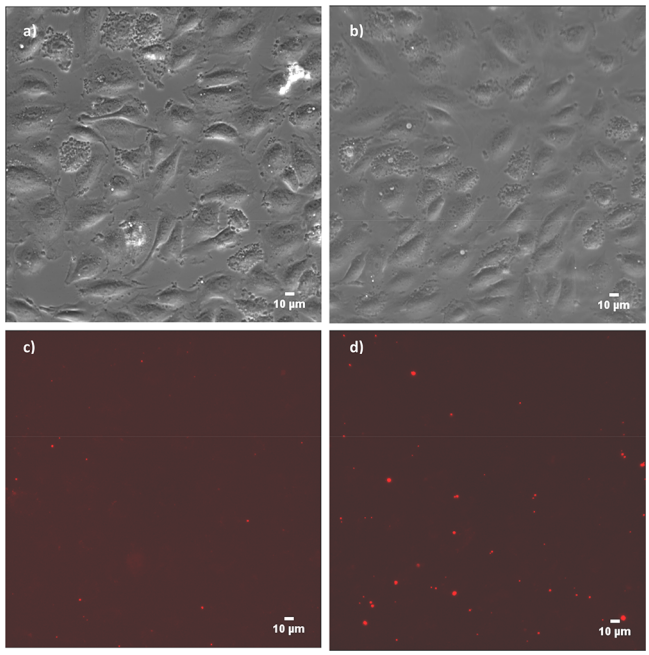

Figure 8. Adhesion of pegylated poly(PCDA) NDs to HUVEC. Micrographs (40×) after 10 min NDs flowing, 5 min inversion, and 10 min PBS washing: (a and c) cells treated with poly(PCDA)-PEG/PFP NDs (control) in bright field and fluorescence microscopy, respectively; (b and d) cells treated with poly(PCDA)PEG-cRGD/PFP in bright field and fluorescence microscopy, respectively.

was then inverted to detach the weakly bound NDs by washing them out with PBS. The persisting cell-bound NDs, considered as the fraction of particles specifically interacting with the cells surface, were subsequently counted and results were normalized to the number of cells present in the ROI. With cRGD conjugated to the surface via PEG spacer, the bioadhesion of NDs is significantly enhanced (0.6 ± 0.15 ND/cell) as compared to the plain poly(PCDA)-PEG/PFP NDs used as control (0.25 ± 0.06 ND/cell). The specificity of bioadhesion to endothelial cells decreases in the case of non-PEGylated poly(PCDA)-cRGD NDs (see Figure S6 in the Supporting Information). As anticipated, the enhanced

DOI: 10.1021/acs.langmuir.9b01160
Langmuir 2019, 35, 10116−10127

targeting efficacy and specificity can be attributed to the flexibility of PEG chains hindering nonspecific bindings and bringing the cRGD moiety attached to the PEG chain end over the accumulated protein corona. These results are promising in the general perspective of an active targeting of poly(PCDA) NDs based on ligand−receptor interaction

4. CONCLUSION

Polymerized PCDA nanodroplets encapsulating low boiling point perfluorocarbon liquids represent a hybrid construct intermediate between lipid and polymer shelled NDs, combining the advantages of both classes of NDs. In this exploratory study optical, acoustic, and ADV properties of this assembly were evaluated as well as cytoxicity and targeting efficacy toward endothelial angiogenic cells. UV curing of the PCDA shell can involve more than 40 diacetylenic molecules on the shell although a study of the factors influencing the radical polymerization, i.e. droplet size, surface curvature as well as curing time, has to be specifically addressed in a future work. We showed that the curing provides a good colloidal stability with both encapsulated PFP and PFB introducing 200 nm^2 patches of 40 polymerized PCDA molecules, dispersed on a monolayer of unbound PCDA molecules. As liquids these perfluorocarbons make the particles active for magnetic resonance detection and represent a reservoir where hydrophobic drug molecules could be dissolved, opening the possibility to used the poly(PCDA) NDs for targeted drug delivery. The same particles once converted into MBs by means of ADV, behave as US contrast agents supporting a dual imaging modality. These results indicate a promising system on the basis of self-assembled and subsequently polymerized diacetylenic particles capable of penetrating the biological barriers based on the nano size of the droplets and the US triggered liquid ↔ gas transition. The characteristics indicate a good potential for the assembly for imaging and drug delivery applications. ADV based systems revert the use of ultrasounds, so far considered almost exclusively the carrier of the diagnostic information. As a consequence, the transformed droplets allow for several options, from already known imaging capability to transport of drugs dissolved in the hydrophobic core of the particles, localized in a tissue area presenting pathology. Formulation of small nanodroplets, smaller than the ones reported here, is possible by tuning the vapor pressure of the PFC core liquid, stirring speed, or sonication power. With such systems made available, the crossing of biological barriers will be feasible and delivery of drug more localized and powerful.

Whether the core phase transition could be triggered by other nonmechanical excitations, as for example by ionizing radiation, has to be investigated. Such a possibility would open the road to the use of NDs as injectable and tumor addressable *in situ* dosimetric devices for personalized medicine.

■ ASSOCIATED CONTENT

Supporting Information

The Supporting Information is available free of charge on the ACS Publications website at DOI: 10.1021/acs.langmuir.9b01160.

Further experimental details, Schemes S1−S4, Figures S1−S7, and Tables S1−S3 as mentioned in the text (PDF)

■ AUTHOR INFORMATION

Corresponding Author

*E-mail: paradossi@stc.uniroma2.it.

ORCID

Fabio Domenici: 0000-0001-6776-2737

Ester Chiessi: 0000-0001-7529-2755

Gaio Paradossi: 0000-0003-3051-3811

Notes

The authors declare no competing financial interest.

■ ACKNOWLEDGMENTS

This work has been partly supported by EU H2020 “AMPHORA”, contract n. 766456.

■ REFERENCES

(1) Dollet, B.; Meer, S. M.; Garbin, V.; Jong, N.; Lohse, D.; Versluis, M. Nonspherical Oscillations of Ultrasound Contrast Agent Microbubbles. *Ultrasound Med. Biol.* **2008**, *34* (9), 1465−1473.

(2) Lee, H. J.; Yoon, T.-J.; Yoon, Y. I. Synthesis of Ultrasound Contrast Agents: Characteristics and Size Distribution Analysis (Secondary Publication). *Ultrason. Ultrason.* **2017**, *36* (4), 378−384.

(3) Unnikrishnan, S.; Klibanov, A. L. Microbubbles as Ultrasound Contrast Agents for Molecular Imaging: Preparation and Application. *AJR, Am. J. Roentgenol.* **2012**, *199* (2), 292−299.

(4) Stride, E.; Saffari, N. Microbubble Ultrasound Contrast Agents: A Review. *Proc. Inst. Mech. Eng., Part H* **2003**, *217* (6), 429−447.

(5) Dijkmans, P. A.; Juffermans, L. J. M.; Musters, R. J. P.; van Wamel, A.; ten Cate, F. J.; van Gilst, W.; Visser, C. A.; de Jong, N.; Kamp, O. Microbubbles and Ultrasound: From Diagnosis to Therapy. *Eur. J. Echocardiogr.* **2004**, *5* (4), 245−246.

(6) Sirsi, S. R.; Borden, M. A. Microbubble Compositions, Properties and Biomedical Applications. *Bubble Sci., Eng., Technol.* **2009**, *1* (1−2), 3−17.

(7) Capece, S.; Domenici, F.; Brasili, F.; Oddo, L.; Cerroni, B.; Bedini, A.; Bordi, F.; Chiessi, E.; Paradossi, G. Complex Interfaces in “Phase-Change” Contrast Agents. *Phys. Chem. Chem. Phys.* **2016**, *18* (12), 8378−8388.

(8) Capece, S.; Chiessi, E.; Cavalli, R.; Giustetto, P.; Grishenkov, D.; Paradossi, G. A General Strategy for Obtaining Biodegradable Polymer Shelled Microbubbles as Theranostic Devices. *Chem. Commun.* **2013**, *49* (51), 5763−5765.

(9) Oddo, L.; Cerroni, B.; Domenici, F.; Bedini, A.; Bordi, F.; Chiessi, E.; Gerbes, S.; Paradossi, G. Next Generation Ultrasound Platforms for Theranostics. *J. Colloid Interface Sci.* **2017**, *491*, 151−160.

(10) Grishenkov, D.; Pecorari, C.; Brismar, T. B.; Paradossi, G. Characterization of Acoustic Properties of PVA-Shelled Ultrasound Contrast Agents: Linear Properties (Part I). *Ultrasound Med. Biol.* **2009**, *35* (7), 1127−1138.

(11) Abou-Saleh, R. H.; Swain, M.; Evans, S. D.; Thomson, N. H. Poly(Ethylene Glycol) Lipid-Shelled Microbubbles: Abundance, Stability, and Mechanical Properties. *Langmuir* **2014**, *30* (19), 5557−5563.

(12) Bjerknes, K.; Sontum, P. C.; Smistad, G.; Agerkvist, I. Preparation of Polymeric Microbubbles: Formulation Studies and Product Characterisation. *Int. J. Pharm.* **1997**, *158* (2), 129−136.

(13) Lentacker, I.; De Geest, B. G.; Vandenbroucke, R. E.; Peeters, L.; Demeester, J.; De Smedt, S. C.; Sanders, N. N. Ultrasound-Responsive Polymer-Coated Microbubbles That Bind and Protect DNA. *Langmuir* **2006**, *22* (17), 7273−7278.

(14) Prajapati, B. G. A. Conceptual Review on Micro Bubbles. *Biomed. J. Sci. Technol. Res.* **2017**, *1* (2), 353−359.

(15) Hernandez, C.; Gulati, S.; Fioravanti, G.; Stewart, P. L.; Exner, A. A. Cryo-EM Visualization of Lipid and Polymer-Stabilized Perfluorocarbon Gas Nanobubbles - A Step Towards Nanobubble

DOI: 10.1021/acs.langmuir.9b01160
Langmuir 2019, 35, 10116−10127

Mediated Drug Delivery. *Sci. Rep.* **2017**, DOI: 10.1038/s41598-017-13741-1.
(16) Martin, K. H.; Dayton, P. A. Current Status and Prospects for Microbubbles in Ultrasound Theranostics: Current Status and Prospects for Microbubbles. *Wiley Interdiscip. Rev. Nanomed. Nanobiotechnol.* **2013**, *5* (4), 329−345.
(17) Kothapalli, S. V. V. N.; Wiklund, M.; Janerot-Sjoberg, B.; Paradossi, G.; Grishenkov, D. Investigation of Polymer-Shelled Microbubble Motions in Acoustophoresis. *Ultrasonics* **2016**, *70*, 275−283.
(18) Lin, C.-Y.; Pitt, W. G. Acoustic Droplet Vaporization in Biology and Medicine. *BioMed Res. Int.* **2013**, *2013*, 1.
(19) Sheeran, P. S.; Matsuura, N.; Borden, M. A.; Williams, R.; Matsunaga, T. O.; Burns, P. N.; Dayton, P. A. Methods of Generating Submicrometer Phase-Shift Perfluorocarbon Droplets for Applications in Medical Ultrasonography. *IEEE Trans. Ultrason. Ferroelectr. Freq. Control* **2017**, *64* (1), 252−263.
(20) Sheeran, P. S.; Luois, S.; Dayton, P. A.; Matsunaga, T. O. Formulation and Acoustic Studies of a New Phase-Shift Agent for Diagnostic and Therapeutic Ultrasound. *Langmuir* **2011**, *27* (17), 10412−10420.
(21) Zhou, Y. Application of Acoustic Droplet Vaporization in Ultrasound Therapy. *J. Ther. Ultrasound* **2015**, DOI: 10.1186/s40349-015-0041-8.
(22) Astafyeva, K.; Somaglino, L.; Desgranges, S.; Berti, R.; Patinote, C.; Langevin, D.; Lazeyras, F.; Salomir, R.; Polidori, A.; Contino-Pépin, C.; et al. Perfluorocarbon Nanodroplets Stabilized by Fluorinated Surfactants: Characterization and Potentiality as Theranostic Agents. *J. Mater. Chem. B* **2015**, *3* (14), 2892−2907.
(23) Rapoport, N. Phase-Shift, Stimuli-Responsive Perfluorocarbon Nanodroplets for Drug Delivery to Cancer: Phase-Shift Perfluorocarbon Nanoemulsions. *Wiley Interdiscip. Rev. Nanomed. Nanobiotechnol.* **2012**, *4* (5), 492−510.
(24) Rapoport, N.; Gao, Z.; Kennedy, A. Multifunctional Nanoparticles for Combining Ultrasonic Tumor Imaging and Targeted Chemotherapy. *JNCI J. Natl. Cancer Inst.* **2007**, *99* (14), 1095−1106.
(25) Chen, C. C.; Sheeran, P. S.; Wu, S. Y.; Olumolade, O. O.; Dayton, P. A.; Konofagou, E. E. Targeted drug delivery with focused ultrasound-induced blood-brain barrier opening using acoustically-activated nanodroplets. *J. Controlled Release* **2013**, *172*, 795−804.
(26) Zhang, X.; Hu, J.; Zhao, G.; Huang, N.; Tan, Y.; Pi, L.; Huang, Q.; Wang, F.; Wang, Z.; Wang, Z.; et al. PEGylated PLGA-Based Phase Shift Nanodroplets Combined with Focused Ultrasound for Blood Brain Barrier Opening in Rats. *Oncotarget* **2017**, *8* (24), 38927−38936.
(27) Wu, S.-Y.; Fix, S. M.; Arena, C.; Chen, C. C.; Zheng, W.; Olumolade, O. O.; Papadopoulou, V.; Novell, A.; Dayton, P. A.; Konofagou, E. E. Focused Ultrasound-Facilitated Brain Drug Delivery Using Optimized Nanodroplets: Vaporization Efficiency Dictates Large Molecular Delivery. *Phys. Med. Biol.* **2018**, *63* (3), 035002.
(28) Cheng, Y.; Dai, Q.; Morshed, R. A.; Fan, X.; Wegscheid, M. L.; Wainwright, D. A.; Han, Y.; Zhang, L.; Auffinger, B.; Tobias, A. L.; et al. Blood-Brain Barrier Permeable Gold Nanoparticles: An Efficient Delivery Platform for Enhanced Malignant Glioma Therapy and Imaging. *Small* **2014**, *10* (24), 5137−5150.
(29) Sykes, E. A.; Chen, J.; Zheng, G.; Chan, W. C. W. Investigating the Impact of Nanoparticle Size on Active and Passive Tumor Targeting Efficiency. *ACS Nano* **2014**, *8* (6), 5696−5706.
(30) Cao, Y.; Chen, Y.; Yu, T.; Guo, Y.; Liu, F.; Yao, Y.; Li, P.; Wang, D.; Wang, Z.; Chen, Y.; et al. Drug Release from Phase-Changeable Nanodroplets Triggered by Low-Intensity Focused Ultrasound. *Theranostics* **2018**, *8* (5), 1327−1339.
(31) Park, Y.; Luce, A. C.; Whitaker, R. D.; Amin, B.; Cabodi, M.; Nap, R. J.; Szleifer, I.; Cleveland, R. O.; Nagy, J. O.; Wong, J. Y. Tunable Diacetylene Polymerized Shell Microbubbles as Ultrasound Contrast Agents. *Langmuir* **2012**, *28* (8), 3766−3772.
(32) Chen, X.; Zhou, G.; Peng, X.; Yoon, J. Biosensors and Chemosensors Based on the Optical Responses of Polydiacetylenes. *Chem. Soc. Rev.* **2012**, *41* (13), 4610−4630.
(33) Guo, C.; Liu, S.; Jiang, C.; Li, W.; Dai, Z.; Fritz, H.; Wu, X. A Promising Drug Controlled-Release System Based on Diacetylene/Phospholipid Polymerized Vesicles. *Langmuir* **2009**, *25* (22), 13114−13119.
(34) Lee, H.-Y.; Tiwari, K. R.; Raghavan, S. R. Biopolymer Capsules Bearing Polydiacetylenic Vesicles as Colorimetric Sensors of PH and Temperature. *Soft Matter* **2011**, *7* (7), 3273−3276.
(35) Chen, Y.-S.; Yoon, S. J.; Frey, W.; Dockery, M.; Emelianov, S. Dynamic Contrast-Enhanced Photoacoustic Imaging Using Photothermal Stimuli-Responsive Composite Nanomodulators. *Nat. Commun.* **2017**, *8*, 15782.
(36) Toumia, Y.; Cerroni, B.; Trochet, P.; Lacerenza, S.; Oddo, L.; Domenici, F.; Paradossi, G. Performances of a Pristine Graphene−Microbubble Hybrid Construct as Dual Imaging Contrast Agent and Assessment of Its Biodistribution by Photoacoustic Imaging. *Part. Part. Syst. Charact.* **2018**, *35* (7), 1800066.
(37) Ishijima, A.; Minamihata, K.; Yamaguchi, S.; Yamahira, S.; Ichikawa, R.; Kobayashi, E.; Iijima, M.; Shibasaki, Y.; Azuma, T.; Nagamune, T.; et al. Selective Intracellular Vaporisation of Antibody-Conjugated Phase-Change Nano-Droplets *in Vitro*. *Sci. Rep.* **2017**, *7*, 44077.
(38) Ho, Y.-J.; Yeh, C.-K. Theranostic Performance of Acoustic Nanodroplet Vaporization-Generated Bubbles in Tumor Intertissue. *Theranostics* **2017**, *7* (6), 1477−1488.
(39) Astafyeva, K.; Somaglino, L.; Desgranges, S.; Berti, R.; Patinote, C.; Langevin, D.; Lazeyras, F.; Salomir, R.; Polidori, A.; Contino-Pépin, C.; et al. Perfluorocarbon Nanodroplets Stabilized by Fluorinated Surfactants: Characterization and Potentiality as Theranostic Agents. *J. Mater. Chem. B* **2015**, *3* (14), 2892−2907.
(40) Rapoport, N. Y.; Nam, K.-H.; Gao, Z.; Kennedy, A. Application of Ultrasound for Targeted Nanotherapy of Malignant Tumors. *Acoust. Phys.* **2009**, *55* (4−5), 594−601.
(41) Fasolato, C.; Giantulli, S.; Silvestri, I.; Mazzarda, F.; Toumia, Y.; Ripanti, F.; Mura, F.; Luongo, F.; Costantini, F.; Bordi, F.; et al. Folate-Based Single Cell Screening Using Surface Enhanced Raman Microimaging. *Nanoscale* **2016**, *8* (39), 17304−17313.
(42) Lange, H.; Rulli, F.; Crestini, C. Gel Permeation Chromatography in Determining Molecular Weights of Lignins: Critical Aspects Revisited for Improved Utility in the Development of Novel Materials. *ACS Sustainable Chem. Eng.* **2016**, *4* (10), 5167−5180.
(43) Zabell, S. L.; Stigler, S. M.; Aldrich, J.; Edwards, A. W. F.; Seneta, E.; Diaconis, P.; Lehmann, E. On Student's 1908 Article "The Probable Error of a Mean" [with Comments, Rejoinder]. *J. Am. Stat. Assoc.* **2008**, *103* (481), 1−20.
(44) Choi, H.; Bae, Y. M.; Yu, G. S.; Huh, K. M.; Choi, J. S. Synthesis of Poly(ethylene glycol)-Polydiacetylene Conjugates and Their Micellar and Chromic Characteristics. *J. Nanosci. Nanotechnol.* **2008**, *8*, 5104−5108.
(45) Yarimaga, O.; Yoon, B.; Ham, D.-Y.; Lee, J.; Hara, M.; Choi, Y.-K.; Kim, J.-M. Electrophoretic Deposition of Amphiphilic Diacetylene Supramolecules: Polymerization, Selective Immobilization, Pattern Transfer and Sensor Applications. *J. Mater. Chem.* **2011**, *21* (46), 18605−18612.
(46) Kim, Y.-H.; Subramanyam, E.; Im, J. H.; Huh, K. M.; Choi, H.; Choi, J. S.; Lee, Y.-K.; Park, S.-W. A New PEG-Lipid Conjugate Micelle for Encapsulation of CdSe/ZnS Quantum Dots. *J. Nanosci. Nanotechnol.* **2010**, *10*, 3275−3279.
(47) Araghi, H. Y.; Paige, M. F. The Effect of Perfluorotetradecanoic Acid on the Structure of Photopolymerized 10,12-Pentacosadiynoic Acid Films at the Air−Water Interface. *Can. J. Chem.* **2013**, *91* (11), 1130−1138.
(48) Vinod, T. P.; Chang, J.-H.; Kim, J.-K.; Rhee, S.-W. Self-Assembly and Photopolymerization of Diacetylene Molecules on Surface of Magnetite Nanoparticles. *Bull. Korean Chem. Soc.* **2008**, *29* (4), 799−804.
(49) Wang, S.; Li, Y.; Shao, L.; Ramirez, J.; Wang, P. G.; Leblanc, R. M. Excess Free Energies of Interaction between 10,12-Pentacosadiynoic Acid (PDA) and Its Mannoside Derivative (MPDA). A Mixed-Monolayer Study. *Langmuir* **1997**, *13* (6), 1677−1681.

DOI: 10.1021/acs.langmuir.9b01160
Langmuir 2019, 35, 10116−10127

(50) Sasaki, D. Y.; Carpick, R. W.; Burns, A. R. High Molecular Orientation in Mono- and Trilayer Polydiacetylene Films Imaged by Atomic Force Microscopy. *J. Colloid Interface Sci.* **2000**, *229* (2), 490−496.
(51) Sheeran, P. S.; Yoo, K.; Williams, R.; Yin, M.; Foster, F. S.; Burns, P. N. More Than Bubbles: Creating Phase-Shift Droplets from Commercially Available Ultrasound Contrast Agents. *Ultrasound Med. Biol.* **2017**, *43* (2), 531−540.
(52) Mountford, P. A.; Borden, M. A. On the Thermodynamics and Kinetics of Superheated Fluorocarbon Phase-Change Agents. *Adv. Colloid Interface Sci.* **2016**, *237*, 15−27.
(53) Sheeran, P. S.; Luois, S. H.; Mullin, L. B.; Matsunaga, T. O.; Dayton, P. A. Design of Ultrasonically-Activatable Nanoparticles Using Low Boiling Point Perfluorocarbons. *Biomaterials* **2012**, *33* (11), 3262−3269.
(54) Reznik, N.; Williams, R.; Burns, P. N. Investigation of Vaporized Submicron Perfluorocarbon Droplets as an Ultrasound Contrast Agent. *Ultrasound Med. Biol.* **2011**, *37* (8), 1271−1279.
(55) Kripfgans, O. D.; Fowlkes, J. B.; Miller, D. L.; Eldevik, O. P.; Carson, P. L. Acoustic Droplet Vaporization for Therapeutic and Diagnostic Applications. *Ultrasound Med. Biol.* **2000**, *26* (7), 1177−1189.
(56) D'Arrigo, J. S.; Imae, T. Physical Characteristics of Ultrastable Lipid-Coated Microbubbles. *J. Colloid Interface Sci.* **1992**, *149* (2), 592−595.
(57) Fabiilli, M. L.; Haworth, K. J.; Fakhri, N. H.; Kripfgans, O. D.; Carson, P. L.; Fowlkes, J. B. The Role of Inertial Cavitation in Acoustic Droplet Vaporization. *IEEE Trans. Ultrason. Ferroelectr. Freq. Control* **2009**, *56* (5), 1006−1017.
(58) Li, H.; Yang, Y.; Zhang, M.; Yin, L.; Tu, J.; Guo, X.; Zhang, D. Acoustic Characterization and Enhanced Ultrasound Imaging of Long-Circulating Lipid-Coated Microbubbles. *J. Ultrasound Med.* **2018**, *37* (5), 1243−1256.
(59) Parrales, M. A.; Fernandez, J. M.; Perez-Saborid, M.; Kopechek, J. A.; Porter, T. M. Acoustic Characterization of Monodisperse Lipid-Coated Microbubbles: Relationship between Size and Shell Viscoelastic Properties. *J. Acoust. Soc. Am.* **2014**, *136* (3), 1077−1084.
(60) Jingqi, W.; Lu, Z.; Jun, Z.; Yuhong, M.; Wei, Y.; Lifeng, R.; Chengbing, J.; Dobromir, D. D.; Hui, Z.; Kun, Z. Clinical Usefulness of the Microbubble Contrast Agent SonoVue in Enhancing the Effects of High-Intensity Focused Ultrasound for the Treatment of Adenomyosis. *J. Ultrasound Med.* **2018**, *37*, 2811.
(61) Ferraioli, G.; Meloni, M. F. Contrast-Enhanced Ultrasonography of the Liver Using SonoVue. *Ultrasonography* **2018**, *37* (1), 25−35.
(62) Harjanto, D.; Lee, J.; Kim, J.-M.; Jaworski, J. Controlling and Assessing the Surface Display of Cell-Binding Domains on Magnetite Conjugated Fluorescent Liposomes. *Langmuir* **2013**, *29* (25), 7949−7956.
(63) Yun, J. S.; Yang, K. S.; Kim, D. H. Multifunctional Polydiacetylene-Graphene Nanohybrids for Biosensor Application. *J. Nanosci. Nanotechnol.* **2011**, *11*, 5663−5669.
(64) Lee, J.; Jun, H.; Kim, J. Polydiacetylene-Liposome Microarrays for Selective and Sensitive Mercury(II) Detection. *Adv. Mater.* **2009**, *21* (36), 3674−3677.
(65) Guo, C.; Liu, S.; Jiang, C.; Li, W.; Dai, Z.; Fritz, H.; Wu, X. A Promising Drug Controlled-Release System Based on Diacetylene/Phospholipid Polymerized Vesicles. *Langmuir* **2009**, *25* (22), 13114−13119.
(66) Veneti, E.; Tu, R. S.; Auguste, D. T. RGD-Targeted Liposome Binding and Uptake on Breast Cancer Cells Is Dependent on Elastin Linker Secondary Structure. *Bioconjugate Chem.* **2016**, *27* (8), 1813−1821.
(67) Meyer, A.; Auernheimer, J.; Kessler, H.; Modlinger, A. Targeting RGD Recognizing Integrins: Drug Development, Biomaterial Research, Tumor Imaging and Targeting. *Curr. Pharm. Des.* **2006**, *12*, 2723−2747.
(68) Wu, P.-H.; Onodera, Y.; Ichikawa, Y.; Rankin, E. B.; Giaccia, A. J.; Watanabe, Y.; Qian, W.; Hashimoto, T.; Shirato, H.; Nam, J.-M. Targeting integrins with RGD-conjugated gold nanoparticles in radiotherapy decreases the invasive activity of breast cancer cells. *Int. J. Nanomed.* **2017**, *12*, 5069−5085.
(69) Garanger, E.; Boturyn, D.; Dumy, P. Tumor Targeting with RGD Peptide Ligands-Design of New Molecular Conjugates for Imaging and Therapy of Cancers. *Anti-Cancer Agents Med. Chem.* **2007**, *7*, 552−558.
(70) Salvati, A.; Pitek, A. S.; Monopoli, M. P.; Prapainop, K.; Bombelli, F. B.; Hristov, D. R.; Kelly, P. M.; Åberg, C.; Mahon, E.; Dawson, K. A. Transferrin-Functionalized Nanoparticles Lose Their Targeting Capabilities When a Biomolecule Corona Adsorbs on the Surface. *Nat. Nanotechnol.* **2013**, *8* (2), 137−143.
(71) Suk, J. S.; Xu, Q.; Kim, N.; Hanes, J.; Ensign, L. M. PEGylation as a Strategy for Improving Nanoparticle-Based Drug and Gene Delivery. *Adv. Drug Delivery Rev.* **2016**, *99*, 28−51.

DOI: 10.1021/acs.langmuir.9b01160
Langmuir 2019, 35, 10116−10127